Short communication

Enhancement of photoelectrochemical response by aligned nanorods in ZnO thin films

Kwang-Soon Ahn[*], Sudhakar Shet, Todd Deutsch, Chun-Sheng Jiang,
Yanfa Yan, Mowafak Al-Jassim, John Turner

National Renewable Energy Laboratory, Golden, CO 80401, USA

Abstract

ZnO thin films are deposited in pure Ar and mixed Ar and N_2 gas ambient at various substrate temperatures by rf sputtering ZnO targets. We find that the deposition in pure Ar ambient leads to polycrystalline ZnO thin films. However, the presence of N_2 in the deposition ambient promotes the formation of aligned nanorods at temperatures above 300 °C. ZnO films with aligned nanorods deposited at 500 °C exhibit significantly enhanced photoelectrochemical response, compared to polycrystalline ZnO thin films grown at the same temperature. Our results suggest that aligned nanostructures may offer potential advantages for improving the efficiency of photoelectrochemical water-splitting for H_2 production.
© 2007 Elsevier B.V. All rights reserved.

Keywords: ZnO nanorod; Gas ambient; Photoelectrochemical; Crystallinity; Bandgap; Sputter

1. Introduction

Transition-metal oxides are attractive candidates for photo-electrochemical (PEC) splitting of water for H_2 production due to their low cost and potential stability [1–4]. However, to date, only TiO_2 has received extensive attention [1,2,5–7]. ZnO has similar bandgap (~3.3 eV) and band-edge positions compared to TiO_2. Furthermore, ZnO has a direct bandgap and higher electron mobility than TiO_2 [8]. Thus, ZnO could also be a potential candidate for PEC splitting of water [9]. However, long-term stability of the ZnO is not good in the acidic and basic solutions under the illumination, which should be overcome by using the protective layers and/or stable dopants.

The performance of thin-film electrodes is often affected by the morphological features of the thin films, such as grain size, grain shape, and surface areas. Thus, electrodes with nanostructures have been applied to improve PEC properties [10–12]. However, most of these nanostructures are not single crystals and are defective. It is known that defects typically act as recombination centers that can kill photon-generated electron–hole pairs before they can reach surfaces and drive reactions. Therefore,

single-crystal nanostructures are highly desirable. For ZnO, various forms of single-crystal nanostructures, such as nanobelts, nanorods, and nanowires, have been reported. The PEC properties of all these nanostructures deserve careful investigation.

In this article, we report on the synthesis and PEC measurements of ZnO thin films sputtered in pure Ar and mixed Ar and N_2 ambient. We find that deposition in pure Ar ambient produces polycrystalline ZnO films, whereas deposition in mixed Ar and N_2 ambient leads to the formation of aligned single-crystal ZnO nanorods along the *c*-axis at temperatures above 300 °C. ZnO films with aligned nanorods grown at 500 °C exhibit significantly enhanced PEC response, compared to polycrystalline ZnO thin films deposited at the same temperature. Our results suggest that the deposition ambient can be used to control the morphology of ZnO thin films and aligned single-crystal nanorods can be potentially beneficial for PEC performance.

2. Experimental

Two sets of samples were deposited. One set was deposited in mixed Ar/N_2 gas ambient. This set of sample is referred to as $ZnO(Ar/N_2)$. The second set of sample was deposited in pure Ar ambient and is referred to as ZnO(Ar). ZnO targets were used in these depositions. Transparent conducting

* Corresponding author. Tel.: +1 303 384 6469; fax: +1 303 384 6491.
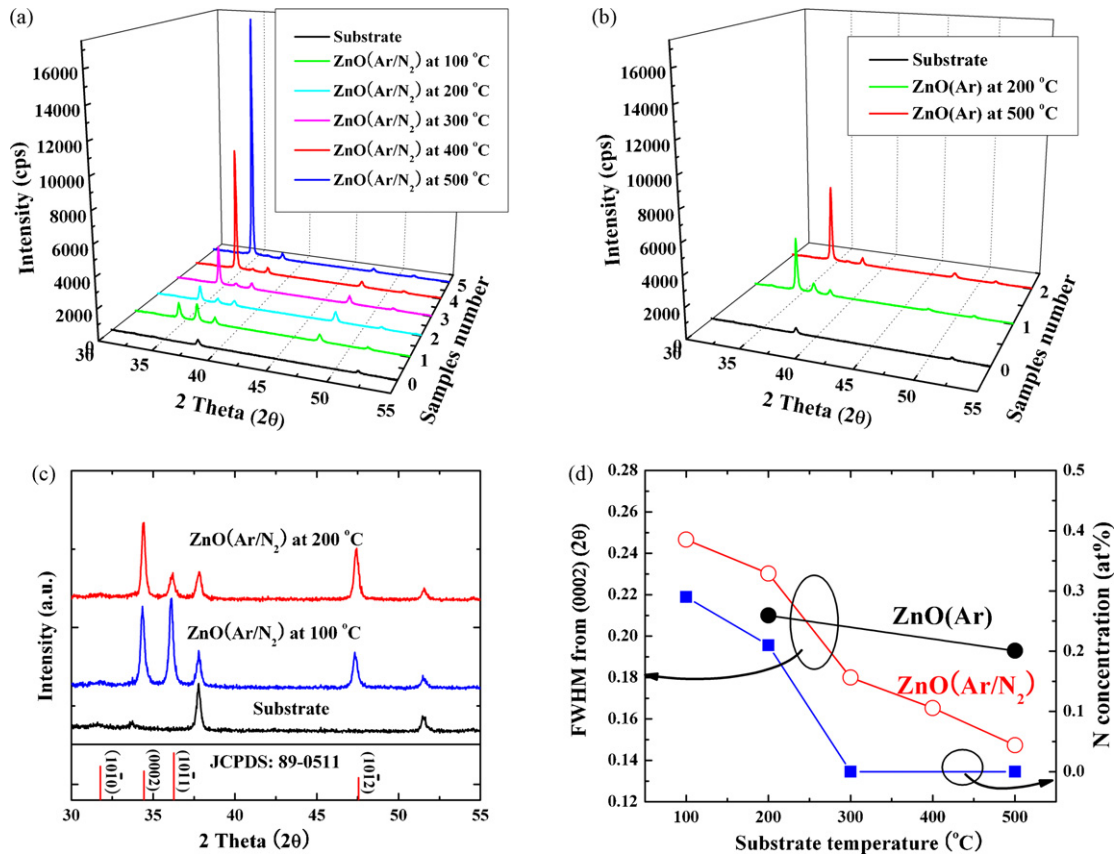*E-mail address:* kwang-soon_ahn@nrel.gov (K.-S. Ahn).

Fig. 1. (Color online) X-ray diffraction curves for (a) $ZnO(Ar/N_2)$ films and (b) $ZnO(Ar)$ films. The sample numbers 1, 2, 3, 4, and 5 along the *y*-axis in (a) correspond to substrate temperature of 100, 200, 300, 400, and 500 °C, and the sample numbers 1 and 2 in (b) correspond to substrate temperatures of 200 and 500 °C. (c) Expanded intensity scale for the substrate and the $ZnO(Ar/N_2)$ films deposited at 100 and 200 °C. (d) FWHM values estimated from (0 0 0 2) for the $ZnO(Ar/N_2)$ and $ZnO(Ar)$ films and the *N* concentrations for the $ZnO(Ar/N_2)$ films as a function of the substrate temperature. (For interpretation of the references to colour in this figure legend, the reader is referred to the web version of the article.)

FTO (20–23 $\Omega\,\square^{-1}$)-coated glass was used as the substrate to allow PEC measurements. The distance between the ZnO target and substrate was about 10 cm, and the substrates were rotated to enhance deposition uniformity. Substrate temperatures were controlled by irradiative Hg lamps and indirectly measured by a thermocouple located below the substrate holder. The base pressure was less than 1×10^{-6} Torr and the working pressure was 5×10^{-3} Torr. The chamber ambient was either pure Ar or mixed Ar and N_2 with gas flow ratio of $N_2/(Ar + N_2) = 5\%$. This low N_2 gas flow ratio was used to obtain a similar deposition rate ($\sim$4.7 nm min^{-1}) with the ZnO(Ar) films, because the deposition rate can also influence film crystallinity. A pre-sputtering cleaning was performed for 20 min to eliminate possible contaminants from the target. Sputtering was conducted at an rf power of 200 W. All the deposited samples were controlled to have similar film thickness of 1 ± 0.05 μm as measured by stylus profilometry.

The structural and crystallinity characterizations were performed by X-ray diffraction (XRD) measurements using an X-ray diffractometer. The *N* concentration in the $ZnO(Ar/N_2)$ films was evaluated by X-ray photoelectron spectroscopy (XPS). The surface morphology was examined by atomic force microscopy (AFM) and field-emission scanning electron microscopy (FE-SEM). The UV–vis absorption spectra of the

samples were measured by an n&k analyzer 1280 (n&k Technology, Inc.) to investigate the optical properties.

PEC measurements were performed in a three-electrode cell with a flat quartz window to facilitate illumination of the photoelectrode surface [13,14]. The sputter-deposited films were used as the working electrodes. A Pt sheet (area: 3 cm × 5 cm) and a Ag/AgCl electrode (with saturated KCl) were used as counter and reference electrodes, respectively. A 0.5-M Na_2SO_4 mild aqueous solution was used as the electrolyte for the stability of the ZnO [14]. Photoelectrochemical response was measured using a fiber-optic illuminator (150-W tungsten-halogen lamp) with a UV/IR cut-off filter (cut-off wavelengths: 350 and 750 nm) and combined UV/IR and green band-pass filter (wavelength: 538.33 nm, full-width at half maximum: 77.478 nm). Light intensity was measured by a photodiode power meter, in which total light intensity with the UV/IR filter was fixed at 125 mW cm^{-2}. The PEC response under light on/off illumination was also measured to confirm the photoresponse of the films during the potential sweep (scan rate = 5 mV s^{-1}).

3. Results and discussion

We first see how the presence of N_2 in the ambient can promote the formation of aligned nanorods in ZnO thin films where
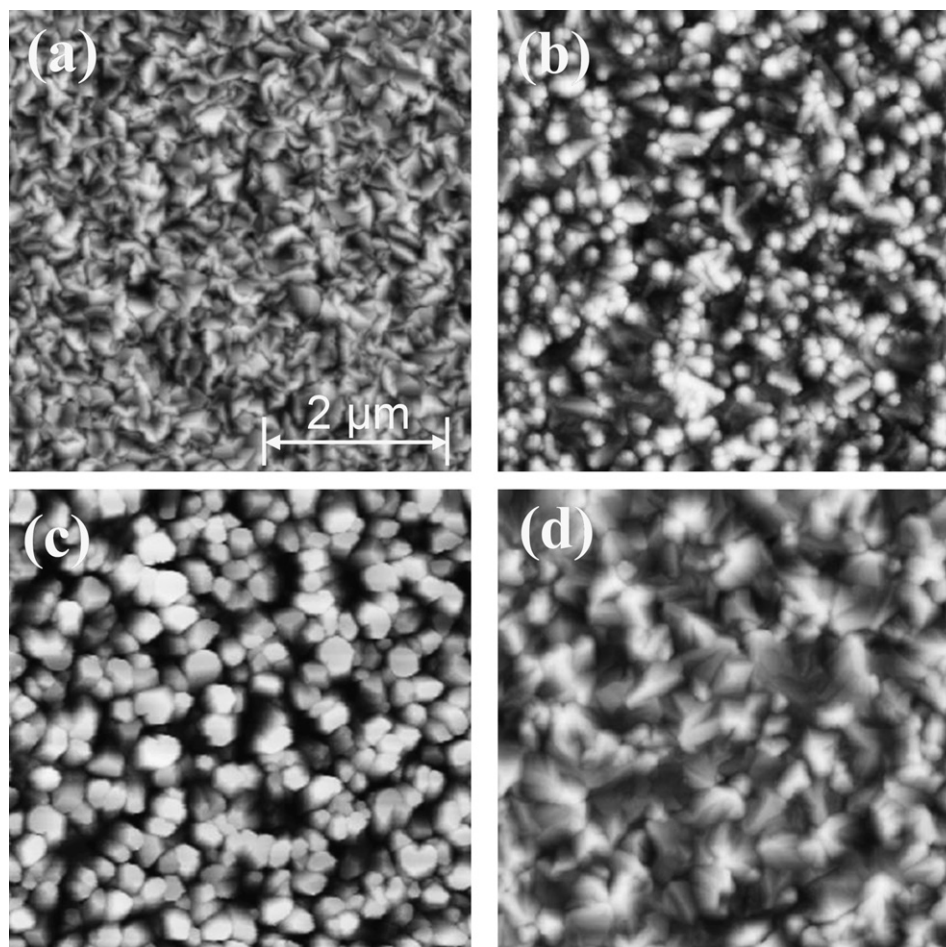
Fig. 2. AFM surface morphology (5 μm × 5 μm) of (a–c) the ZnO(Ar/N$_2$) films deposited at the substrate temperatures of 100, 400, and 500 °C, respectively, and (d) the ZnO(Ar) film deposited at 500 °C.

the substrate temperature is higher than 300 °C. Fig. 1(a) and (b) shows XRD curves for the ZnO(Ar/N$_2$) films and ZnO(Ar) films deposited at different substrate temperatures. The crystallinity of ZnO films increases gradually with the increase of substrate temperatures in both cases. Fig. 1(c) shows the expanded intensity scale for the substrate and ZnO(Ar/N$_2$) films deposited at 100 and 200 °C. These two ZnO(Ar/N$_2$) films have random orientation. With the increase of substrate temperature to 500 °C, the (0 0 0 2) peak of the ZnO(Ar/N$_2$) film was enhanced greatly, as shown in Fig. 1(a). The measured full-width at half-maximum (FWHM) values of (0 0 0 2) peaks are shown in Fig. 1(d). The N concentrations (at.%) for the ZnO(Ar/N$_2$) films measured by XPS are also given in Fig. 1(d). With the increase of substrate temperature, the N concentration decreased rapidly and disappeared at temperatures above 300 °C. The FWHM of ZnO(Ar) decreased slightly with the increase of substrate temperature. ZnO(Ar/N$_2$) films grown at temperatures below 200 °C exhibited random orientation and larger FWHM values than the ZnO(Ar) films grown at the same temperatures. This is because the high concentration of N is incorporated in ZnO(Ar/N$_2$) films at these temperatures. It is known from recent reports that incorporated N atoms can deteriorate the crystal structure and modify the growth mode [15–17]. However, the FWHM values of ZnO(Ar/N$_2$) films decrease rapidly when the substrate

temperatures are above 300 °C because no significant N can be incorporated at these temperatures. At substrate temperatures above 300 °C, ZnO(Ar/N$_2$) films exhibit much smaller FWHM values than the ZnO(Ar) films. The rapid growth of the FWHM values indicates either increased crystallinity or formation of nanorods or nanowires along the c-axis.

AFM images reveal that the significantly increased (0 0 0 2) peak in the XRD curve obtained in ZnO(Ar/N$_2$) at 500 °C is largely due to the formation of aligned nanorods along the c-axis. Fig. 2 shows AFM surface morphology (5 μm × 5 μm) of the ZnO(Ar/N$_2$) films deposited at the substrate temperatures of 100, 400, and 500 °C (Fig. 2(a)–(c), respectively), and the ZnO(Ar) film deposited at 500 °C (Fig. 2(d)). It shows clearly that the ZnO(Ar/N$_2$) film deposited at 100 °C has a random orientation. As substrate temperature increases, aligned nanorods along the c-axis are favored to form. At 500 °C, the ZnO(Ar/N$_2$) film reveals the growth of hexagonal-like nanorods. However, the ZnO(Ar) film deposited at the same temperature is polycrystalline (Fig. 2(d)). It should be noted that at 500 °C, the diameters of the nanorods are smaller than that of the grains in polycrystalline ZnO film. The smaller FWHM value for the ZnO(Ar/N$_2$) film is attributed to the nanorod feature [18–20].

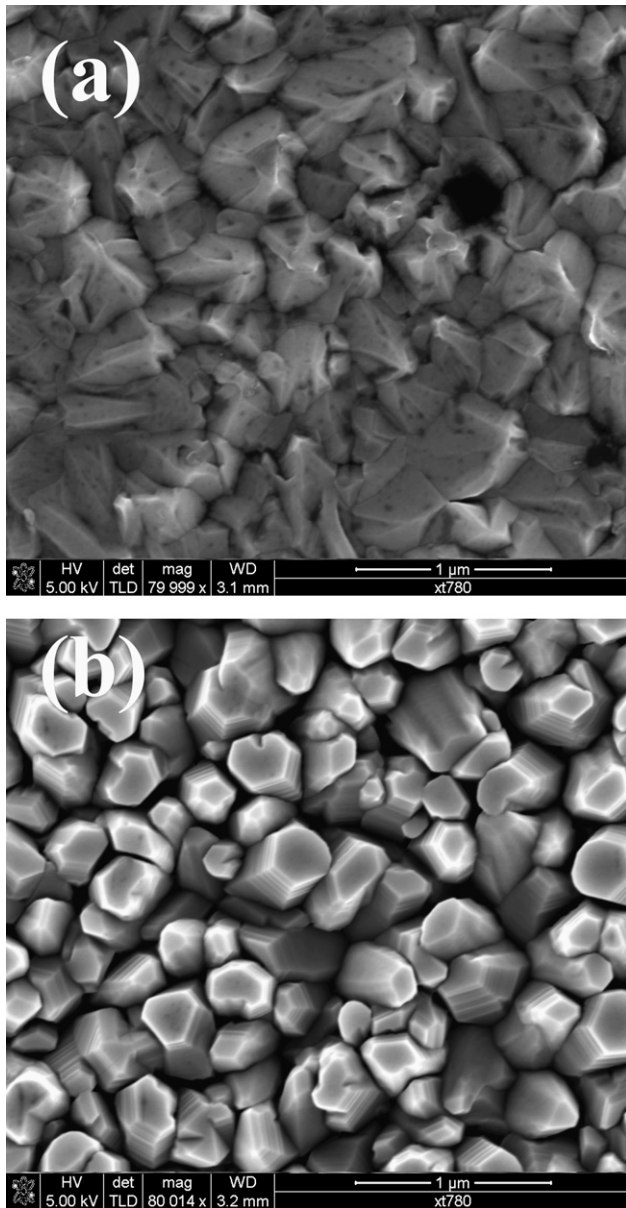Fig. 3(a) and (b) shows FE-SEM top-views of the ZnO(Ar) and ZnO(Ar/N$_2$) films, respectively, deposited at a substrate

Fig. 3. FE-SEM top-views of the (a) ZnO(Ar) film and (b) ZnO(Ar/N₂) nanorod film, respectively, deposited at 500 °C.

Fig. 4. (Color online) (a) Absorption coefficients for the ZnO(Ar/N₂) and ZnO(Ar) films deposited at different substrate temperatures. (b) Estimated optical bandgaps of ZnO(Ar/N₂) and ZnO(Ar) films as a function of the substrate temperature. (For interpretation of the references to colour in this figure legend, the reader is referred to the web version of the article.)

temperature of 500 °C. It clearly shows that the nanorod structure was not present in the ZnO(Ar) film, whereas the ZnO(Ar/N₂) films at 500 °C exhibited vertically aligned, single-crystal hexagonal-like nanorods with flat (0 0 0 2) surfaces. No metal clusters were found at the end of the nanorods, indicating that the growth mechanism is not the catalyst-assisted vapor–liquid–solid (VLS) growth [19–21]. Recently, catalyst-free ZnO nanorods/nanowires have been synthesized by various chemical and physical techniques such as plasma-enhanced chemical vapor deposition, metal-organic vapor-phase epitaxy, and pulsed laser deposition [19–22]. The nanorod structures provide high surface areas and superior carrier transport (or conductivity) along the c-axis, which may lead to increased interfacial reaction sites and reduced recombination rate [10,23]. Therefore, the aligned nanorod
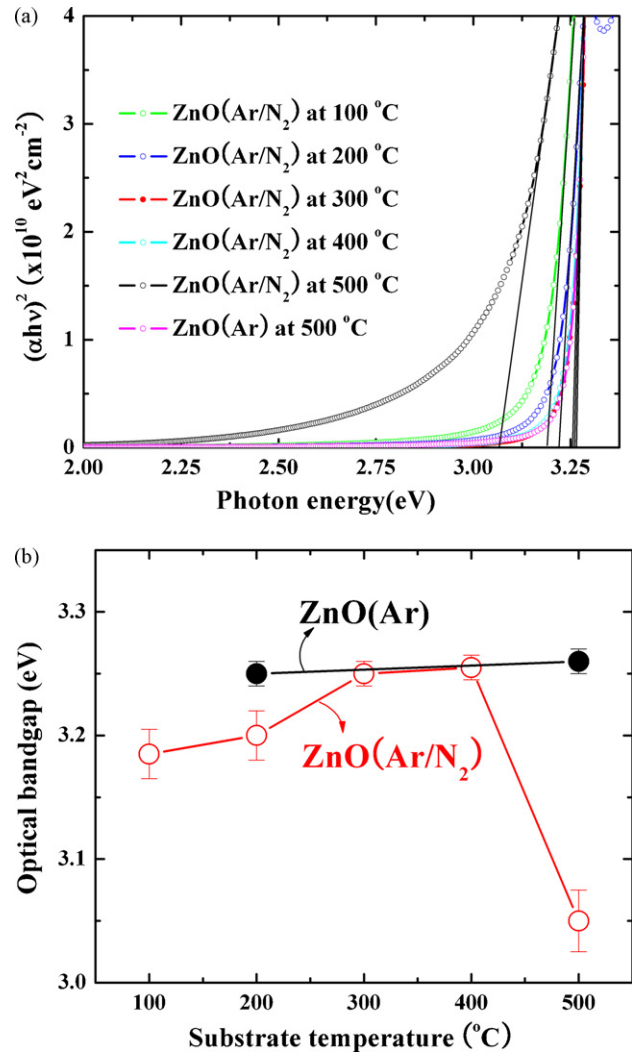
films deposited at 500 °C should lead to enhanced PEC response.

We have also measured the optical absorption coefficients for these ZnO films. Because ZnO has a direct bandgap, the optical bandgap can be described by the following equation [17]:

$$(\alpha h \nu)^2 = \beta (h\nu - E_g), \qquad (1)$$

where $h\nu$ is the photon energy, E_g is an optical bandgap, and β is the edge width. The absorption coefficient (α) was calculated by the following equation [17]:

$$\alpha = -\frac{1}{d} \ln\left(\frac{T}{1-R}\right), \qquad (2)$$

where d is the film thickness and R and T are the measured reflectance and transmittance, respectively. Fig. 4(a) shows absorption coefficients of the ZnO(Ar/N₂) and ZnO(Ar) films deposited at different substrate temperatures. The direct optical bandgaps of the films were determined by extrapolating the

linear portion of each curve in Fig. 4(a) to $(\alpha h v)^2 = 0$, with the resulting values plotted in Fig. 4(b). The measured optical bandgaps for ZnO(Ar) films deposited at 200 and 500 °C are almost the same (about 3.26 eV) [24]. The bandgap of the ZnO(Ar/N$_2$) film deposited at 100 °C is 3.19 eV, lower than that of the ZnO(Ar) films. This bandgap reduction is due to the incorporation of N, which generates an impurity band above the valance band of ZnO [2,25]. However, when substrate temperatures are increased to 300 and 400 °C, the bandgap reduction disappears. It is because at these temperatures, N incorporation is suppressed, as confirmed by XPS composition measurements (Fig. 1(d)). Thus, the bandgaps of ZnO(Ar/N$_2$) grown at these temperatures should have similar bandgaps as the ZnO(Ar) films. It is interesting to note, however, that the ZnO(Ar/N$_2$) films with aligned nanorods deposited at 500 °C exhibited a much lower bandgap (3.05 eV) than the ZnO(Ar) film grown at the same temperature. Because XPS indicates no detectable N incorporated in the ZnO(Ar/N$_2$) nanorod film, the bandgap reduction must be induced by intrinsic defects, likely oxygen vacancies [26], which could explain the absorption tail below 3 eV. The impurity band can enable light absorption in the long-wavelength regions.

The PEC response for the ZnO films deposited in different ambient was also investigated. Fig. 5(a) and (b) shows photocurrent–voltage curves of the ZnO(Ar/N$_2$) and ZnO(Ar) films deposited at 500 °C, respectively, under continuous illumination (red curve), dark condition (black curve), and light on/off illumination (blue curve) with an UV/IR filter. Both ZnO films show very small dark currents up to a potential of 1.4 V. The ZnO(Ar/N$_2$) nanorod film deposited at 500 °C exhibited much higher photocurrents than the ZnO(Ar) film deposited at the same substrate temperature.

To see the effects of substrate temperature on PEC response, we measured photocurrent at a 1.2 V potential for ZnO(Ar/N$_2$) and ZnO(Ar) films under continuous illumination with UV/IR filter. Fig. 6(a) shows the measured photocurrents as a function of the substrate temperature for the ZnO(Ar/N$_2$) and ZnO(Ar) films. At low substrate temperatures (below 300 °C), the photocurrents of ZnO(Ar/N$_2$) films are similar to that of ZnO(Ar) films, although these ZnO(Ar/N$_2$) films have smaller bandgaps than ZnO(Ar) films. For these ZnO(Ar/N$_2$) samples, low crystallinity (Fig. 1(d)) could be responsible for the small photocurrents because the photocurrent increases for ZnO(Ar/N$_2$) films as the substrate temperature increases, as does the crystallinity. The ZnO(Ar/N$_2$) film deposited at 500 °C exhibits the best photoelectrochemical response—more than two times higher than the ZnO(Ar) films deposited at the same temperature. The enhancement can be attributed to the aligned nanorod structure along the c-axis and additional light absorption in the long-wavelength regions. The electron–hole pairs are generated by the absorption of photons with energies larger than the bandgap and separated by the electric field of the depletion region. In the case of n-type semiconductors, the excited electrons move through bulk region to the counter electrode where water reduction occurs. The generated holes move towards semiconductor/electrolyte interface where water oxidation takes place. The aligned nanorod structures along the c-axis
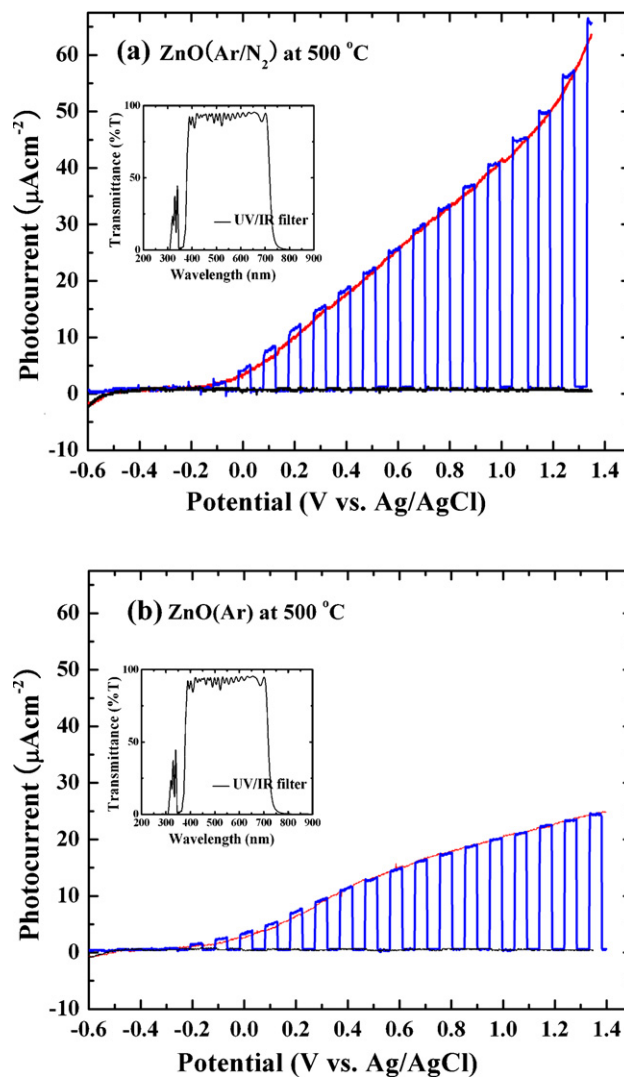

Fig. 5. (Color online) Photocurrent–voltage curves of (a) ZnO(Ar/N$_2$) nanorod and (b) ZnO(Ar) films, deposited at 500 °C under (red curve) continuous illumination, (black curve) dark condition, and (blue curve) light on/off illumination with an UV/IR filter. Electrolyte and scan rate were 0.5 M Na$_2$SO$_4$ mild aqueous solution and 5 mV s^{-1}, respectively. (For interpretation of the references to colour in this figure legend, the reader is referred to the web version of the article.)

provide high surface area and superior carrier transport along the c-axis, leading to the increased interfacial reaction sites and reduced recombination rate between the electrons and holes. As a result, the PEC performance of the nanorod structure is greatly enhanced.

To investigate the photoresponse of the ZnO(Ar/N$_2$) nanorod films deposited at 500 °C in the long-wavelength regions, a green color filter was used in combination with the UV/IR filter. For comparison, PEC responses for ZnO(Ar) films deposited at 500 °C were also measured and are shown in Fig. 6(b). The ZnO(Ar) films exhibit no clear photoresponse due to their large bandgaps. On the other hand, the ZnO(Ar/N$_2$) nanorod films show considerable photocurrents in the long-wavelength regions (green filter). These currents can only be due to photon absorption by the defect bands. Thus, our results indicate
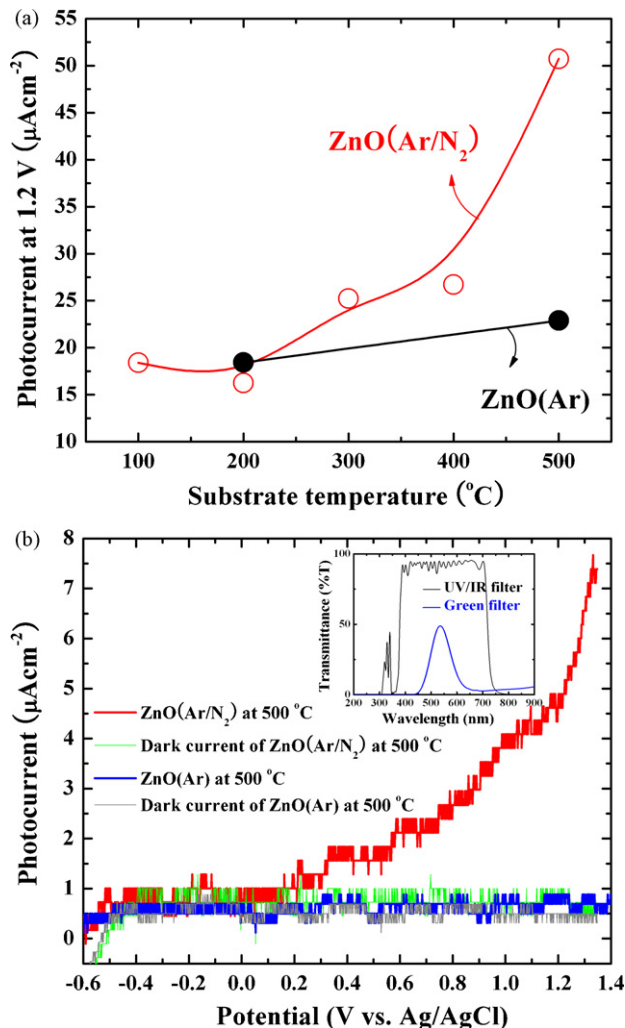
Fig. 6. (Color online) (a) Photocurrents measured at 1.2 V as a function of the substrate temperature for the ZnO(Ar/N$_2$) and ZnO(Ar) films. (b) Photocurrent–voltage curves of ZnO(Ar/N$_2$) nanorod and ZnO(Ar) films deposited at 500 °C under illumination using combined UV/IR and green filters. (For interpretation of the references to colour in this figure legend, the reader is referred to the web version of the article.)

that the formation of impurity bands do not necessarily significantly increase the recombination rate and can be used to provide additional photon absorption in the long-wavelength regions. It should be pointed out, however, that the concentration of point defects should be optimized. If the concentration is too high, the point defects may significantly increase the electron–hole recombination rate and act as dominant recombination centers, resulting in the decreased photoresponse. This has been seen in the low-crystallinity ZnO(Ar/N$_2$) films deposited below 300 °C. Nonetheless, our results show that sputter-deposited ZnO films at the substrate temperature of 500 °C in mixed Ar/N$_2$ gas ambient exhibited aligned nanorods along the c-axis and slightly reduced bandgap, leading to greatly enhanced PEC response.

4. Conclusions

We have investigated the structural properties, optical absorption, and PEC responses for ZnO deposited at different temperatures by sputtering the ZnO target in pure Ar gas and mixed Ar/N$_2$ gas ambient. We found that the presence of N$_2$ in the growth ambient helps to promote the formation of aligned nanorods and impurity bands at a high substrate temperature of 500 °C, resulting in the significantly enhanced PEC response, compared to ZnO(Ar) films deposited in pure Ar gas ambient. Our results suggest that deposition ambient can be used to produce desired properties of thin films, and aligned nanorods may help to improve PEC performance.

Acknowledgements

References

[1] A. Fujishima, K. Honda, Nature 238 (1972) 37.
[2] R. Asahi, T. Morikawa, T. Ohwaki, K. Aoki, Y. Taga, Science 293 (2001) 269.
[3] O. Khaselev, J.A. Turner, Science 280 (1998) 425.
[4] V.M. Aroutiounian, V.M. Arakelyan, G.E. Shahnazaryan, Solar Energy 78 (2005) 581.
[5] J. Yuan, M. Chen, J. Shi, W. Shangguan, Int. J. Hydrogen Energy 31 (2006) 1326.
[6] G.K. Mor, K. Shankar, M. Paulose, O.K. Varghese, C.A. Grimes, Nano Lett. 5 (2005) 191.
[7] B. O'Regan, M. Grätzel, Nature 353 (1991) 737.
[8] K. Kakiuchi, E. Hosono, S. Fujihara, J. Photochem. Photobiol. A: Chem. 179 (2006) 81.
[9] T.F. Jaramillo, S.H. Baeck, A. Kleiman-Shwarsctein, E.W. McFarland, Macromol. Rapid Commun. 25 (2004) 297.
[10] C.M. López, K.-S. Choi, Chem. Commun. (2005) 3328.
[11] J.B. Baxter, E.S. Aydil, Sol. Energy Mater. Sol. Cells 90 (2006) 607.
[12] M. Grätzel, Nature 414 (2001) 338.
[13] K.-S. Ahn, S.-H. Lee, A.C. Dillon, C.E. Tracy, R. Pitts, J. Appl. Phys. 101 (2007) 093524.
[14] K.-S. Ahn, Y. Yan, S.-H. Lee, T. Deutsch, J. Turner, C.E. Tracy, C. Perkins, M. Al-Jassim, J. Electrochem. Soc. 154 (2007) B956.
[15] X. Li, Y. Yan, T.A. Gessert, C.L. Perkins, D. Young, C. DeHart, M. Young, T.J. Coutts, J. Vac. Sci. Technol. A 21 (2003) 1342.
[16] C. Jagadish, S.J. Pearton, Zinc Oxide Bulk, Thin Films and Nanostructures, Elsevier, Amsterdam, 2006 (Chapter 3).
[17] D. Paluselli, B. Marsen, E.L. Miller, R.E. Rocheleau, Electrochem. Solid-State Lett. 8 (2005) G301.
[18] Y. Li, X. Li, C. Yang, Y. Li, J. Mater. Chem. 13 (2003) 2641.
[19] X. Liu, X. Wu, H. Cao, R.P.H. Chang, J. Appl. Phys. 95 (2004) 3141.
[20] W.I. Park, D.H. Kim, S.-W. Jung, G.-C. Yi, Appl. Phys. Lett. 80 (2002) 4232.
[21] S. Choopun, H. Tabata, T. Kawai, J. Cryst. Growth 274 (2005) 167.
[22] F. Xu, Z.-Y. Yuan, G.-H. Du, T.-Z. Ren, C. Bouvy, M. Halasa, B.-L. Su, Nanotechnology 17 (2006) 588.
[23] M. Law, L.E. Greene, J.C. Johnson, R. Saykally, P. Yang, Nat. Mater. 4 (2005) 455.
[24] C.X. Xu, X.W. Sun, X.H. Zhang, L. Ke, S.J. Chua, Nanotechnology 15 (2004) 856.
[25] K.-S. Ahn, Y. Yan, M. Al-Jassim, J. Vac. Sci. Technol. B 25 (4) (2007) L23.
[26] S. Dutta, S. Chattopadhyay, D. Jana, A. Banerjee, S. Manik, S.K. Pradhan, M. Sutradhar, A. Sarkar, J. Appl. Phys. 100 (2006) 114328.